ISSN 2078-5615. Вісник Львівського університету. Серія хімічна. 2026. Випуск 67. С. 228–241
Visnyk of the Lviv University. Series Chemistry. 2026. Issue 67. P. 228–241

UDC 544.43

KINETICS OF THE FORMATION OF Ni–Fe BIMETALLIC NANOPARTICLES

L. Bazylyak[1,2*], Ya. Pilyuk[1], I. Halatyn[1], A. Fedorchuk[1], A. Kytsya[1,2]

[1]*Department of Physical Chemistry of Fossil Fuels*
of the Institute of Physical Organic Chemistry and Coal Chemistry
named after L. M. Lytvynenko NAS Ukraine,
Naukova Str. 3a, 79060 Lviv, Ukraine
[*]*e-mail: bazylyak.liliya@gmail.com*;

[2]*Karpenko Physico-Mechanical Institute of the NAS of Ukraine,*
Naukova Str., 5, 79060, Lviv, Ukraine

The effect of the initial precursor concentrations and temperature on the kinetics of formation of bimetallic Ni–Fe nanoparticles (Ni_xFe_{100-x}–NPs) was investigated. It was shown that the kinetic curves exhibit an S-shaped profile, indicating the autocatalytic nature of the process. It was established that: (1) the nucleation and growth rates of Ni_xFe_{100-x}–NPs slightly increase with decreasing nickel content in the reaction mixture from 100 to 80 % and decrease after the iron content in the system reaches 25 %; (2) the activation energy of bimetallic nanoparticle nucleation does not depend on the fraction of iron ions in the reaction mixture and is almost twice as high as the activation energy of Ni_xFe_{100-x}–NPs growth. The elemental and phase compositions of the Ni_xFe_{100-x}–NPs were examined. A formation mechanism for Ni_xFe_{100-x}–NPs is proposed, involving nucleation via partial dissolution of nickel hydroxide in the presence of hydrazine followed by the formation of $[Ni(N_2H_4)_x]^{2+}$ complex, its decomposition, and the generation of zero-valent nickel; catalytic decomposition of hydrazine yielding highly reactive intermediates; and nanoparticle growth via decomposition of the nickel–hydrazine complex and interaction of hydrazine decomposition intermediates with insoluble $Fe(OH)_2$.

Keywords: kinetics, nanoparticles, nickel, iron.

DOI: https://doi.org/10.30970/vch.6701.228

1. Introduction

The rapid development of radio-electronic technologies over the past decades has led to an extremely high level of environmental pollution by electromagnetic radiation (EMR). In particular, currently the level of electromagnetic radiation is millions of times higher than the natural level that was established during the development of biosystems [1]. Such a high level of electromagnetic pollution of the environment affects not only the performance of radio-electronic devices and appliances, but also negatively affects human health [2]. Thus, reducing the harmful effects of EMF is a relevant interdisciplinary problem today. In the last decade, a significant amount of research has been devoted to protecting radio-electronic devices from the effects of high- and ultra-high-frequency electromagnetic radiation. One of the most effective ways to protect against EMF is to use special screens, in particular those based on polymer nanostructured materials. The effectiveness of EMI shielding by such materials is determined by a complex of factors,

among which the specific electrical conductivity and magnetic permeability of the fillers play a key role. In particular, the penetration depth of an electromagnetic wave, at which its intensity is decreased by approximately in 3 times, is inversely proportional to the specific electrical conductivity and magnetic permeability of the material [3].

In this regard, promising fillers for composite materials for protective purposes are electrically conductive and magnetically active nanostructured materials, primarily based on metals and their alloys [4–8]. It is the nanoscale state of such fillers allows to combine the high values of electrical conductivity and magnetic permeability with the possibility of the formation of percolation networks in the polymer matrix at relatively low filler concentrations. At the same time, nanostructures based on ferromagnetic metals, in particular iron, cobalt, and nickel [9–13], are of particular interest, which is due to their high values of magnetic permeability, which in some cases provide the EMF attenuation at a level of up to 150 dB/mm [14]. Therefore, the search for new electrically conductive, in particular nanostructured, fillers for composite materials is an urgent scientific and applied problem.

A promising direction is the use of polymetallic, in particular bimetallic, nanostructures, since the combination of two metals within one nanosystem makes it possible to purposefully vary their electrical and magnetic characteristics, as well as influence the morphology, particle size, and stability of properties in the composite. In particular, bimetallic systems based on nickel and iron combine the high magnetic permeability of iron with the good electrical conductivity and corrosion properties of nickel, which makes them promising fillers for polymer materials for protective purposes.

An important stage in the development and optimization of methods for obtaining the polymetallic nanopowders is the study of the kinetic patterns of the processes of nucleation and growth of a new phase. Therefore, the purpose of this work stage was to investigate the effect of initial precursor concentrations and temperature on the kinetics of the formation of bimetallic nanosystems Ni_xFe_{100-x}.

2. Materials and experimental methods

The kinetics of the reduction reaction of metal ions with hydrazine was studied by the volumetric method, since the reduction of metal ions with hydrazine in an alkaline medium is occurred according to the gross reaction (1), which is accompanied by the catalytic decomposition of hydrazine (2, 3).

$$2M^{2+} + 4OH^- + N_2H_4 = 2M^0 + 4H_2O + N_2\uparrow \quad (1)$$

$$N_2H_4 \xrightarrow{M} N_2\uparrow + 2H_2\uparrow \quad (2)$$

$$3N_2H_4 \xrightarrow{M} N_2\uparrow + 4NH_3\uparrow \quad (3)$$

Ni_xFe_{100-x} nanoparticles (Ni_xFe_{100-x}–NPs) of various compositions were synthesized by the reduction reaction of a mixture of the corresponding salts with hydrazine in the presence of sodium hydroxide in an ethylene glycol medium in a sealed quartz reactor with a thermostatic jacket, equipped with a magnetic stirrer and an injector for adding the reagents, which was connected to a bottle with a lower tube filled with water (Fig. 1). As a result of the reaction, a gas mixture (N_2 + H_2) is evaluated, which displaces water from the system. Accordingly, the volume of evaluated gas was recorded by the volume of displaced water.

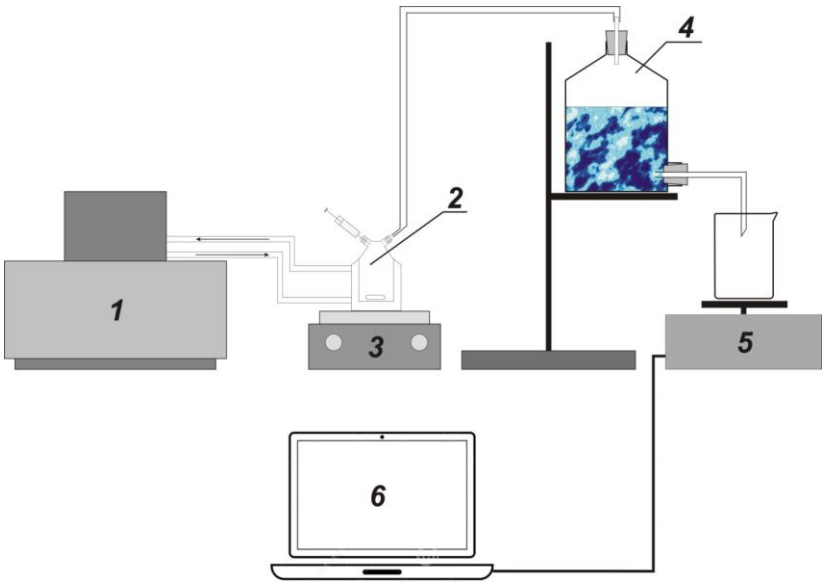

Fig. 1. Schematic diagram of the setup for studying the kinetics of bimetallic nanoparticles formation. Here: *1* – circulation thermostat; *2* – reactor with thermostatic jacket and injector; *3* – magnetic stirrer; *4* – bottle with a bottom tube; *5* – electronic scale; *6* – personal computer

The completion of the reaction was indicated by the formation of a black precipitate. The nanoparticles were separated from the reaction medium using a neodymium magnet, washed with distilled water, and dried under reduced pressure.

The elemental composition of the synthesized nanoparticles was studied using an EVO–40XVP scanning electron microscope (Carl Zeiss) equipped with an INCA Energy 350 energy-dispersive X-ray microanalysis system.

The structure of Ni_xFe_{100-x}–NPs was studied by X-ray powder diffraction using DRON–3.0 and Aeris–Malvern Panalytical diffractometers (Cu–Kα radiation).

3. Results and discussion

The study of the influence of the ratio of nickel and iron ions in the reaction mixture on the kinetics of the formation of bimetallic Ni–Fe nanoparticles was carried out in a water / ethylene glycol medium at their volume ratio of 1/5 under the following conditions: t = 70 °C, ν(Ni+Fe) = 0.0025 mole, ν(NaOH) = 0.05 mole, ν(N_2H_4) = 0.2 mole, V = 60 ml, mixer speed is 500 min^{-1}.

It was found that the kinetic curves of the process consist of 3 sections (Fig. 2, *a*): I) induction period of the reaction; II) rapid gas evolution via reaction (1), i. e. reduction of metal ions – the growth process of Ni_xFe_{100-x}–NPs; III) the decomposition of an excess of the hydrazine, catalyzed by Ni_xFe_{100-x}–NPs.

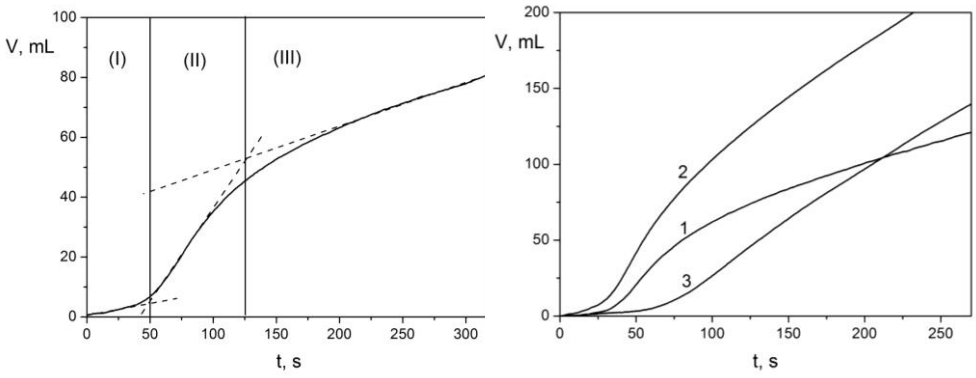

a *b*

Fig. 2. Kinetic curves of the gas mixture evolution during the synthesis of Ni-NPs (*a*) and Ni_xFe_{100-x}–NPs (*b*) for the Ni : Fe molar ratios in the reaction mixtures: *1* – 90 : 10; *2* – 75 : 25; *3* – 50 : 50

The process parameters were calculated from the kinetic curves: the duration of the induction period (t_{ind}), which is inversely proportional to the nucleation rate, the rate of gas evolution during the reduction of metal ions (dV/dt(*max*)), and the rate of catalytic decomposition of hydrazine (dV/dt(N_2H_4)). The gas evolution rates at each stage of the process were determined by the tangents of the angles of inclination to the straight-line sections of the kinetic curves (Fig. 2, *a*). It should be noted that for each of the experimental conditions, at least three kinetic curves were recorded, and the calculated kinetic parameters were averaged, which increased the reliability of the obtained results.

It was established (Table 1) that the duration of the induction period is slightly decreased with a decrease of the nickel content in the reaction mixture from 100 to 80 % at. and is increased after reaching the Fe content in the system to 25 % at. The values dV/dt(*max*) and dV/dt(N_2H_4) (Fig. 3, *a*) also is changed non-monotonously.

Table 1

Duration of the induction period and the values of the rate of gas mixture evolution at different stages of Ni_xFe_{100-x}–NPs formation at different ratios of elements in the reaction mixture

Ni : Fe, % at.	t_{ind}, s	dV/dt(*max*), mL/s	dV/dt(N_2H_4), mL/s	W_g, mL/s
100 : 0	46 ± 5	0.7±0.2	0.17±0.02	0.53
90 : 10	45 ± 5	1.2±0.2	0.36±0.09	0.84
80 : 20	30 ± 6	1.8±0.1	0.7±0.1	1.1
75 : 25	32 ± 3	1.7±0.2	0.8±0.1	0.9
70 : 30	45 ± 15	1.8±0.1	1.1±0.1	0.7
60 : 40	50 ± 5	1.3±0.1	1.1±0.1	0.2
50 : 50	80 ± 20	0.73±0.04	0.6±0.1	0.13
40 : 60	140 ± 30	0.36±0.02	0.34±0.05	0.02

As can be seen from Fig. 3, the rate of catalytic decomposition of hydrazine monotonously is increased with an increase of the part of Fe in the system up to 30 %. This may probably be due to the increased contribution of reaction (3) to the N_2H_4 decomposition process.

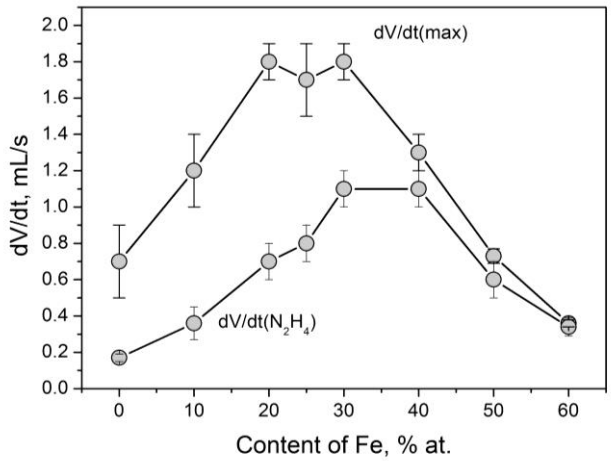

Fig. 3. Dependences of gas evolution rates during the reduction of metal ions and catalytic decomposition of hydrazine on the part of Fe in the reaction mixture

Considering the methodology of kinetic studies, it should be noted that the value of V, which is fixed experimentally, is the sum of the volumes of gases evaluated via reactions (1)–(3). Thus, the value of dV/dt(*max*) inaccurately characterizes the growth rate of Ni_xFe_{100-x}–NPs. Accordingly, to estimate the growth rate (W_g) of Ni_xFe_{100-x}–NPs, the value of the gas evolution rate in section (II) of the kinetic curve (Fig. 2, *a*) was used calculated via the equation.

$$W_g = dV/dt(max) - dV/dt(N_2H_4) \quad (4)$$

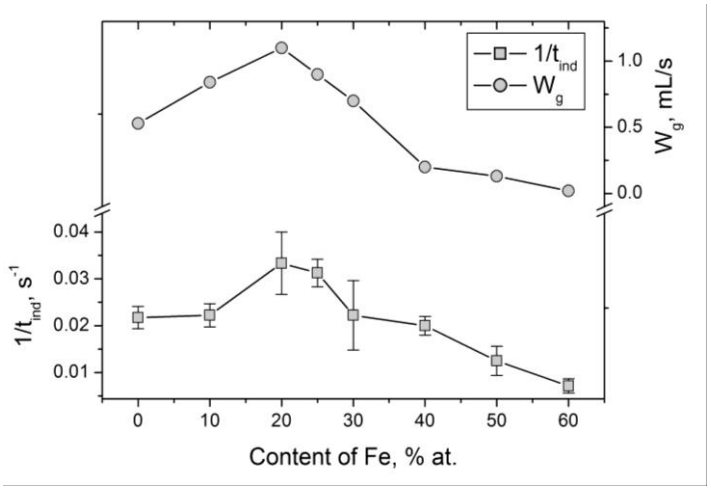

Fig. 4. Dependences of the nucleation rates ($1/t_{ind}$) and growth rates (W_g) of Ni_xFe_{100-x}–NPs on the part of Fe in the reaction mixture

As can be seen from Fig. 4, the changes in the nucleation and growth rates of Ni_xFe_{100-x}–NPs correlate well with each other. With an increase in the Fe content till 20 %, $1/t_{ind}$ and W_g are increased slightly, and after an increase of the Fe content above 25 %, they are decreased. This can probably be explained as follows. In the Fe–Ni system at low (below 400 °C) temperatures, the formation of intermetallic compounds of the composition $FeNi_3$, FeNi, and Fe_3Ni was detected. Moreover, according to "The Open Quantum Materials Database (OQMD)" [15, 16], the value of the enthalpy of formation (ΔH_f) of $FeNi_3$ is the lowest (Fig. 5) and is equal to –0.09 eV/at (–8.5 kJ/mol).

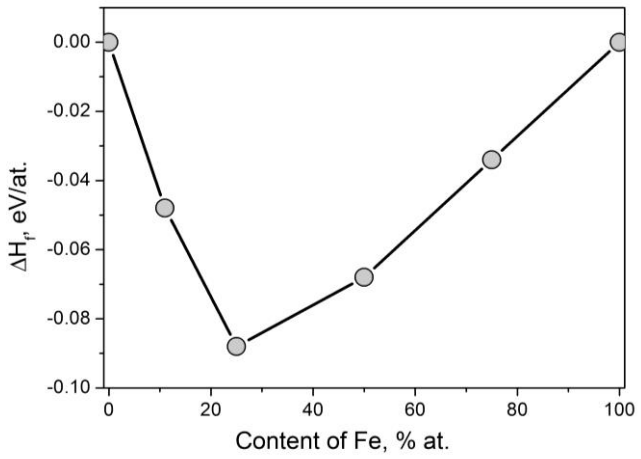

Fig. 5. Dependence of the enthalpies of formation of Ni_xFe_{100-x} on the composition (according to OQMD data)

That is, it can be assumed that the nucleus of a new phase in this system will be the $FeNi_3$ phase.

In order to establish the activation parameters of the process, the effect of temperature on the rate of formation of bimetallic nanosystems Ni_xFe_{100-x} was investigated. The study was conducted under the following initial conditions: ν(Ni + Fe) = 0.0003 mole; ν(Ni + Fe) = 0.0003 mole; x = 100, 70, 30; ν(NaOH) = 0.0125 mole; $\nu(N_2H_4)$ = 0.05 mole; mix rate – 500 min^{-1}. Before adding the hydrazine, the reaction mixture was bubbled with nitrogen for 15 min.

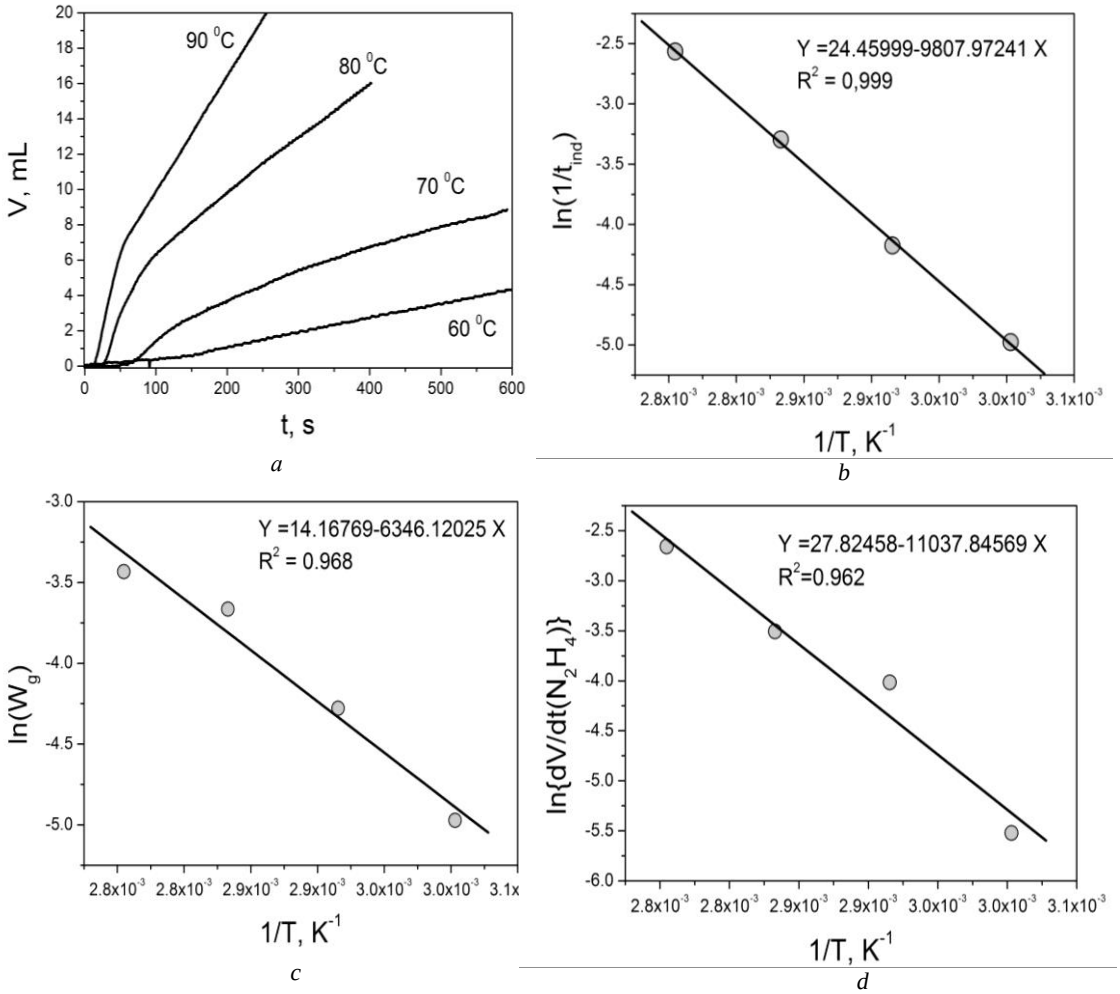

Fig. 6. Kinetic curves of the gas mixture evolution during the synthesis of Ni-NPs at different temperatures (*a*) and the dependencies of the rates of nucleation (*b*), growth of Ni-NPs (*c*) and catalytic decomposition of hydrazine (*d*) on temperature in the *Arrhenius* coordinates

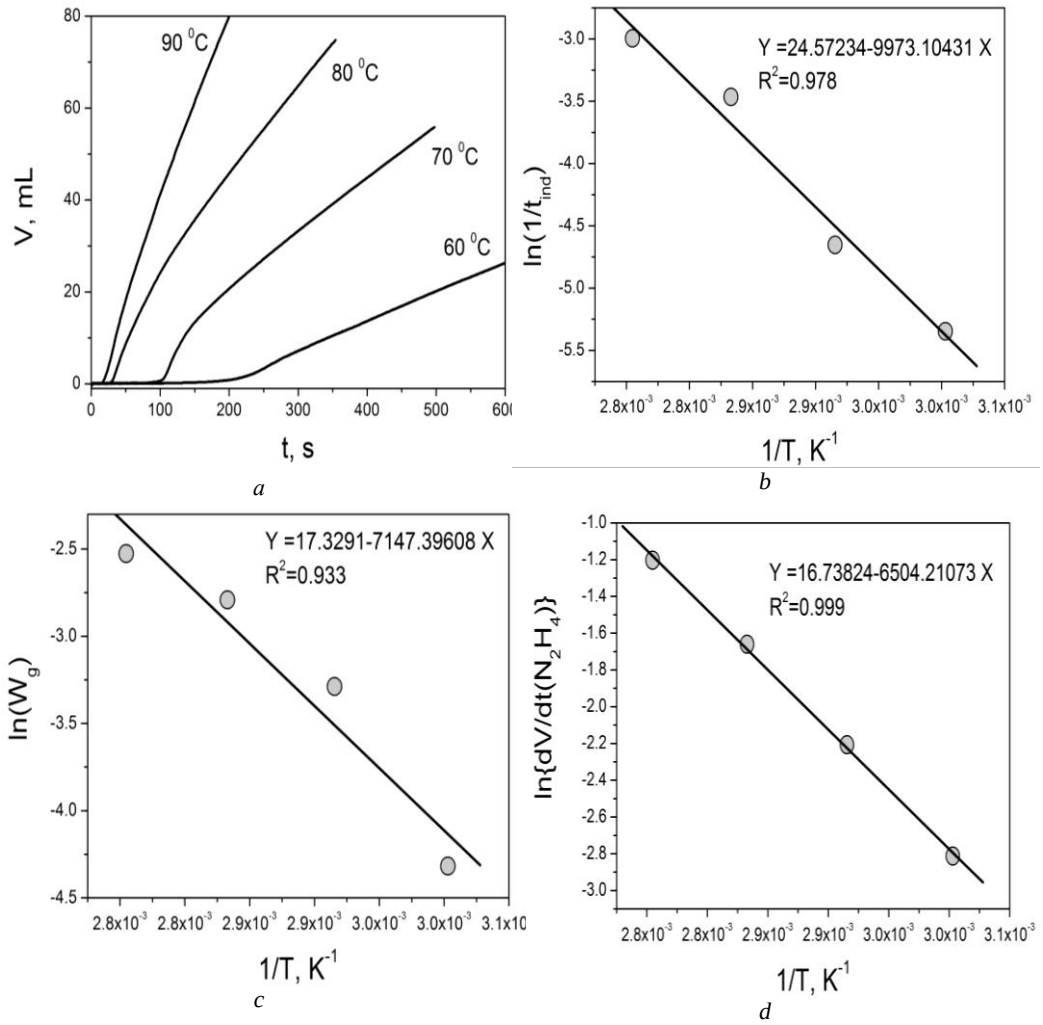

Fig. 7. Kinetic curves of the gas mixture evolution during the synthesis of $Ni_{70}Fe_{30}$ at different temperatures (*a*) and the dependencies of the rates of nucleation (*b*), growth of $Ni_{70}Fe_{30}$ (*c*) and catalytic decomposition of hydrazine (*d*) on temperature in the *Arrhenius* coordinates

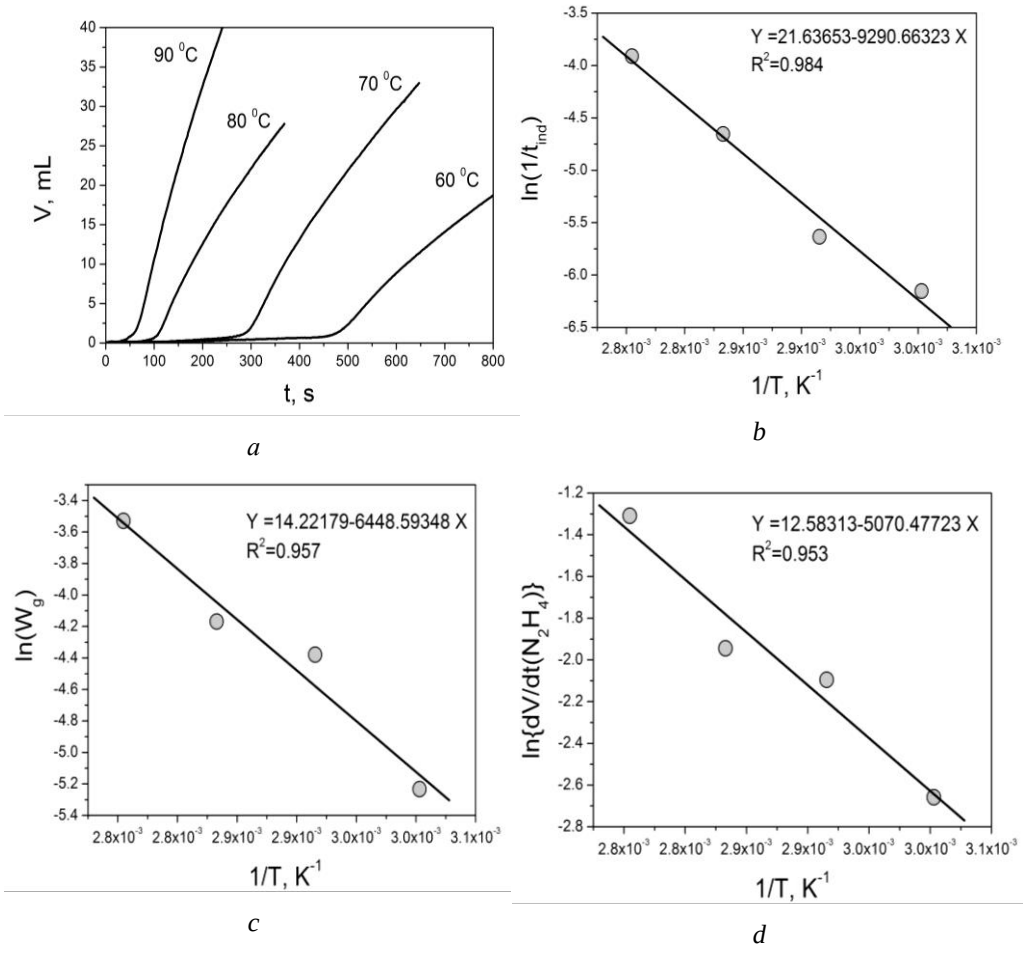

a *b*

c *d*

Fig. 8. Kinetic curves of the gas mixture evolution during the synthesis of $Ni_{50}Fe_{50}$ at different temperatures (*a*) and the dependencies of the rates of nucleation (*b*), growth of $Ni_{50}Fe_{50}$ (*c*) and catalytic decomposition of hydrazine (*d*) on temperature in the *Arrhenius* coordinates

It was found (Table 2) that the values of the activation energies of nucleation ($E_A(N)$) and growth ($E_A(G)$) of Ni_xFe_{100-x} nanoparticles for the all studied cases are practically the same, which indicates the similarity of the mechanisms of these processes regardless of the part of Fe^{2+} ions in the reaction mixture. At the same time, the activation energy of the catalytic decomposition of hydrazine ($E_A(N_2H_4)$) is decreased with a decrease of the part of nickel ions in the system. Thus, it can be assumed that the decomposition of hydrazine in the presence of Ni_{100} is occurred according to the reaction (2). Conversely, in the cases of Ni–Fe bimetallic nanoparticles, the catalytic decomposition of N_2H_4 is occurred according to the reaction (3).

Table 2

Activation parameters of Ni_xFe_{100-x}–NPs formation at different element ratios in the reaction mixture

Ni : Fe, % at.	$E_A(N)$, kJ/mole	$E_A(G)$, kJ/mole	$E_A(N_2H_4)$, kJ/mole
100 : 0	81.5 ± 2.5	52.7 ± 6.7	92± 13
70 : 30	82.9 ± 8.9	59.4 ± 11.3	54.0 ± 1.4
50 : 50	77.2 ± 7.1	53.6 ± 8.0	42.1 ± 6.5

In order to establish the influence of synthesis conditions on the properties of the obtained nanoparticles, the elemental and phase composition of individual Ni_xFe_{100-x}–NPs samples was investigated.

It was found (Table 3) that the Ni : Fe ratio in the obtained Ni_xFe_{100-x}–NPs is in satisfactory agreement with the ratio of the elements in the initial reaction mixture. At the same time, with an increase of the part of iron, an increase of the oxygen content is observed.

Table 3

Element composition of Ni_xFe_{100-x}–NPs

Ni : Fe, % at.	Content, % at.		
	Ni	Fe	O
100 : 0	96.9	—	3.1
75 : 25	66.4	22.7	10.9
50 : 50	33.6	34.5	31.9

Using the X-ray powder diffraction method, it was established (Fig. 9) that the obtained $Ni_{75}Fe_{25}$–NPs and $Ni_{50}Fe_{50}$–NPs contain an oxide phase of Fe_3O_4 (spinel type) and a metallic phase based on nickel and iron (Cu type).

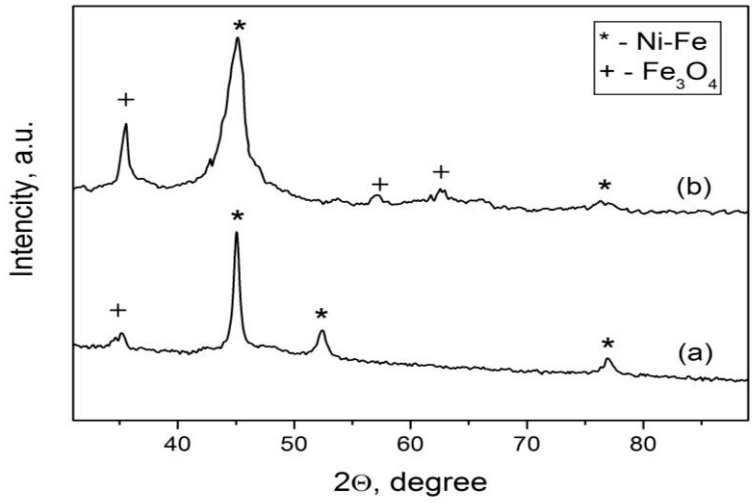

Fig. 9. XRD patterns of $Ni_{75}Fe_{25}$–NPs (*a*) and $Ni_{50}Fe_{50}$–NPs (*b*)

The obtained results indicate an oxidation of nanoparticles during the washing, drying, and preparation of samples for research. The low corrosion resistance of Ni_xFe_{100-x}–NPs with a high iron content is also indicated by the change in the color of the samples from black to brown-brown during their storage at room conditions.

Considering that the solubility of freshly prepared $Ni(OH)_2$ is an order of magnitude higher than that of $Fe(OH)_2$, and the stability constants of $[Ni(N_2H_4)_x]^{2+}$ complexes are higher compared to those for iron [17], we can assume the following scheme of formation of Ni_xFe_{100-x}–NPs. The formation of nuclei is occurred due to the partial dissolution of nickel hydroxide in the presence of hydrazine and due to the formation of the complex $[Ni(N_2H_4)_x]^{2+}$ with subsequent decomposition of the complex and reduction of Ni^{2+} to the zero-valent metal. After the formation of nuclei, the decomposition of the "nickel–hydrazine" complex and the catalytic decomposition of hydrazine is occurred in parallel, during which highly reactive intermediate products are formed (reactions 5–9) [18], which can interact with insoluble $Fe(OH)_2$ with the formation of zero-valent iron.

$$N_2H_4 \rightarrow 2\ NH_2^{\bullet} \quad (5)$$

$$NH_2^{\bullet} + N_2H_4 \rightarrow NH_3 + N_2H_3^{\bullet} \quad (6)$$

$$2\ N_2H_3^{\bullet} \rightarrow N_2H_4 + N_2H_2 \quad (7)$$

$$2\ N_2H_2 \rightarrow N_2H_4 + N_2 \quad (8)$$

$$2\ N_2H_3^{\bullet} \rightarrow N_4H_6 \rightarrow 2NH_3 + N_2 \quad (9)$$

That is, it can be assumed that the obtained Ni_xFe_{100-x}–NPs are heterogeneous and a gradient of iron content can be observed in individual particles – from a low in the center of the particle to high on the outside, similar to bimetallic Cu–Ni nanoparticles [19]. This assumption is in good agreement with the results of elemental and phase analysis of the samples: the XRD patterns lack peaks characteristic of nickel oxide, i. e. only the iron is oxidized.

At the same time, the relatively low oxygen content in the $Ni_{75}Fe_{25}$ sample may support the assumption of the formation of nuclei of the $FeNi_3$ phase composition, but this assumption requires additional experimental confirmation.

4. Conclusions

It was found that the nucleation and the growth rates of Ni–Fe nanoparticles (Ni_xFe_{100-x}–NPs) are slightly increased with a decrease of the nickel content in the reaction mixture from 100 to 80 % and are increased after reaching the Fe content of 25 % in the system. It was found that the activation energy of the nucleation of bimetallic nanoparticles does not depend on the part of iron ions in the reaction mixture and is almost twice as high as the activation energy of the growth of Ni_xFe_{100-x}–NPs. A scheme for the formation of Ni_xFe_{100-x}–NPs is proposed, which includes the formation of nuclei due to the partial dissolution of nickel hydroxide in the presence of hydrazine and the formation of the $[Ni(N_2H_4)_x]^{2+}$ complex with its subsequent decomposition and the formation of zero-valent nickel; catalytic decomposition of hydrazine with the formation of highly reactive intermediate products; growth of nanoparticles due to the decomposition of the nickel–hydrazine complex and the interaction of hydrazine decomposition intermediates with insoluble $Fe(OH)_2$.

1. *Kyzymchuk O. P., Arabuli S. I., Vlasenko V. I.* Textile materials for protection against electromagnetic radiation // Visnyk KNUTD. 2019. Vol. 3, No. 134. P. 48–61 (in Ukrainian). DOI: https://doi.org/10.30857/1813-6796.2019.3.5

2. *Kovalenko V. V., Tykhenko O. M., Levchenko L. O.* Priority directions of work on protection of workers from the influence of electromagnetic radiation of ultra-high and extremely high frequencies // Visnyk KrNU. 2016. Vol. 5, No. 100. P. 82–86 (In Ukrainian).
3. *Chung D. D.* Materials for electromagnetic interference shielding // J. Mater. Eng. Perform. 2000. Vol. 9, No. 3. P. 350–354. DOI: https://doi.org/10.1361/105994900770346042
4. *Huang C. Y., Wu C. C.* The EMI shielding effectiveness of PC/ABS/nickel-coated carbon fibre composites // Eur. Polym. J. 2000. Vol. 36, No. 12. P. 2729–2737. DOI: https://doi.org/10.1016/S0014-3057(00)00039-2
5. *Yang Y., Gupta M. C., Dudley K. L.* Studies on electromagnetic interference shielding characteristics of metal nanoparticle- and carbon nanostructure-filled polymer composites in the Ku-band frequency // Micro Nano Lett. 2007. Vol. 2, No. 4. P. 85–89. DOI: https://doi.org/10.1049/mnl:20070042
6. *Aswathi M. K., Rane A. V., Ajitha A. R., Thomas S., Jaroszewski M.* EMI shielding fundamentals // Advanced Materials for Electromagnetic Shielding: Fundamentals, Properties, and Applications. 2018. P. 1–9. DOI: https://doi.org/10.1002/9781119128625.ch1
7. *Das S., Sharma S., Yokozeki T., Dhakate S.* Conductive layer-based multifunctional structural composites for electromagnetic interference shielding // Compos. Struct. 2021. Vol. 261. Art. 113293. DOI: https://doi.org/10.1016/j.compstruct.2020.113293
8. *Sankaran S., Deshmukh K., Ahamed M. B., Pasha S. K.* Recent advances in electromagnetic interference shielding properties of metal and carbon filler reinforced flexible polymer composites: a review // Compos. Part A: Appl. Sci. Manuf. 2018. Vol. 114. P. 49–71. DOI: https://doi.org/10.1016/j.compositesa.2018.08.006
9. *Joseph N., Sebastian M. T.* Electromagnetic interference shielding nature of PVDF–carbonyl iron composites // Mater. Lett. 2013. Vol. 90. P. 64–67. DOI: https://doi.org/10.1016/j.matlet.2012.09.014
10. *Gargama H., Thakur A. K., Chaturvedi S. K.* Polyvinylidene fluoride / nanocrystalline iron composite materials for EMI shielding and absorption applications // J. Alloys Compd. 2016. Vol. 654. P. 209–215. DOI: https://doi.org/10.1016/j.jallcom.2015.09.059
11. *Kumar R., Choudhary H. K., Anupama A. V., Menon A. V., Pawar S. P., Bose S., Sahoo B.* Nitrogen doping as a fundamental way to enhance the EMI shielding behavior of cobalt particle-embedded carbonaceous nanostructures // New J. Chem. 2019. Vol. 43, No. 14. P. 5568–5580. DOI: https://doi.org/10.1039/C9NJ00639G
12. *Zhao H., Hou L., Bi S., Lu Y.* Enhanced X-band electromagnetic-interference shielding performance of layer-structured fabric-supported polyaniline/cobalt–nickel coatings // ACS Appl. Mater. Interfaces. 2017. Vol. 9, No. 38. P. 33059–33070. DOI: https://doi.org/10.1021/acsami.7b07941
13. *Shukla V.* Review of electromagnetic interference shielding materials fabricated by iron ingredients // Nanoscale Adv. 2019. Vol. 1, No. 5. P. 1640–1671. DOI: https://doi.org/10.1039/C9NA00108E
14. *Gao H., Wang C., Yang Z., Zhang Y.* 3D porous nickel metal foam/polyaniline heterostructure with excellent electromagnetic interference shielding capability and superior absorption based on pre-constructed macroscopic conductive framework // Compos. Sci. Technol. 2021. Vol. 213. Art. ID 108896. DOI: https://doi.org/10.1016/j.compscitech.2021.108896

15. *Saal J. E., Kirklin S., Aykol M., Meredig B., Wolverton C.* Materials design and discovery with high-throughput density functional theory: the Open Quantum Materials Database (OQMD) // JOM. 2013. Vol. 65. P. 1501–1509. DOI: https://doi.org/10.1007/s11837-013-0755-4
16. *Kirklin S., Saal J. E., Meredig B., Thompson A., Doak J. W., Aykol M., Wolverton C.* The Open Quantum Materials Database (OQMD): assessing the accuracy of DFT formation energies // npj Comput. Mater. 2015. Vol. 1. Art. 15010. DOI: https://doi.org/10.1038/npjcompumats.2015.10
17. *Audrieth L. F., Ogg B. A.* The Chemistry of Hydrazine. John Wiley & Sons. New York, 1951.
18. *Grinberg D. A., Moore K. B., Jasper A. W., Green W. H. Jr.* Large intermediates in hydrazine decomposition: a theoretical study of the N_3H_5 and N_4H_6 potential energy surfaces // J. Phys. Chem. A. 2019. Vol. 123, No. 22. P. 4679–4692. DOI: https://doi.org/10.1021/acs.jpca.9b02217
19. *Kytsya A. R., Bazylyak L. I., Zavaliy I. Y., Verbovytskyy Y. V., Zavalij P.* Synthesis, structure and hydrogenation properties of Ni–Cu bimetallic nanoparticles // Appl. Nanosci. 2022. DOI: https://doi.org/10.1007/s13204-021-01742-6

КІНЕТИЧНІ ЗАКОНОМІРНОСТІ ФОРМУВАННЯ БІМЕТАЛЕВИХ НАНОЧАСТИНОК Ni-Fe

Л. Базиляк[1,2*], **Я. Пілюк**[1], **І. Галатин**[1], **А. Федорчук**[1], **А. Киця**[1,2]

[1]*Відділення фізико-хімії горючих копалин*
Інституту фізико-органічної хімії і вуглехімії ім. Л. М. Литвиненка
Національної академії наук України
вул. Наукова, 3а, 79060. Львів, Україна
[*]*e-mail: bazylyak.liliya@gmail.com;*

[2]*Фізико-механічний інститут ім. Г. В. Карпенка*
Національної академії наук України
вул. Наукова, 5, *79060, м. Львів, Україна*

Перспективним напрямом застосування біметалевих наночастинок на основі феромагнітних металів є створення композиційних матеріалів для захисту радіоелектронних засобів від електромагнітних випромінювань високих і надвисоких частот. Зокрема, біметалеві наносистеми на основі нікелю та заліза поєднують високу магнітну проникність заліза з добрими електропровідними та корозійностійкими властивостями нікелю, що зумовлює їх перспективність як наповнювачів полімерних матеріалів захисного призначення. У зв'язку з цим актуальним є розроблення економічно доцільних методів синтезу біметалевих наночастинок Ni–Fe прогнозованого складу.

Важливим етапом створення та оптимізації методів одержання поліметалевих наночастинок є дослідження кінетичних закономірностей процесів зародження та росту нової фази. Досліджено вплив вихідних концентрацій прекурсорів і температури на кінетику формування біметалевих наночастинок Ni–Fe (Ni_xFe_{100-x}–NPs). Показано, що кінетичні криві їх формування мають S-подібний характер, що свідчить про автокаталітичну природу процесу.

З'ясовано, що:

1) швидкості зародження та росту Ni_xFe_{100-x}–NPs дещо зростають зі зменшенням вмісту нікелю в реакційній суміші від 100 до 80 % та знижуються після досягнення вмісту заліза в системі 25 %;

2) енергія активації зародження біметалевих наночастинок не залежить від частки іонів заліза в реакційній суміші та є майже вдвічі вищою, порівняно з енергією активації росту Ni_xFe_{100-x}–NPs.

Досліджено елементний і фазовий склад Ni_xFe_{100-x}–NPs. Показано, що співвідношення Ni : Fe в одержаних нанопорошках задовільно узгоджується зі складом вихідної реакційної суміші. Водночас зі збільшенням частки заліза простежується зростання вмісту кисню, а сформовані Ni_xFe_{100-x}–NPs містять оксидну фазу Fe_3O_4 та металеву фазу на основі нікелю та заліза. Запропоновано схему формування Ni_xFe_{100-x}–NPs, яка містить утворення зародків внаслідок часткового розчинення гідроксиду нікелю за наявності гідразину з подальшим утворенням комплексу $[Ni(N_2H_4)_x]^{2+}$, його розкладом і формуванням нуль-валентного нікелю; каталітичний розклад гідразину з утворенням високореакційних проміжних продуктів; ріст наночастинок унаслідок розкладу комплексу "нікель–гідразин" і взаємодії інтермедіатів розкладу гідразину з нерозчинним $Fe(OH)_2$.

Ключові слова: кінетика, наночастинки, нікель, залізо.

Стаття надійшла до редколегії 30.10.2025
Після доопрацювання 20.01.2026
Прийнята до друку 12.02.2026
Оприлюднена онлайн 29.05.2026